HHS Public Access

Author manuscript

J Mol Biol. Author manuscript; available in PMC 2019 October 19.

Published in final edited form as:

J Mol Biol. 2018 October 19; 430(21): 4036–4048. doi:10.1016/j.jmb.2018.07.029.

Biochemical and structural insights into an Fe(II)/α-ketoglutarate/O_2 dependent dioxygenase, Kdo 3-hydroxylase (KdoO)

Sang Hoon Joo[#a,b], **Charles W. Pemble IV**[#c,d], **Eun Gyeong Yang**[e], **Christian R. H. Raetz**[a], and **Hak Suk Chung**[a,e,f,*]

[a]Duke University Medical Center, Department of Biochemistry, Durham, 27710, USA

[b]Department of Pharmacy, Daegu Catholic University, Gyeongbuk 38430, South Korea

[c]Duke Macromolecular Crystallography Center, Duke University Medical Center, Durham, North Carolina 27710, USA.

[d]Human Vaccine Institute, Duke University Medical Center, Durham, North Carolina 27710, USA

[e]Center for Theragnosis, Biomedical Research Institute, Korea Institute of Science and Technology, Seoul 02792, Republic of Korea

[f]Division of Bio-Medical Science & Technology, KIST School, Korea University of Science and Technology, Seoul 02792, Republic of Korea

[#] These authors contributed equally to this work.

Abstract

During lipopolysaccharide (LPS) biosynthesis in several pathogens, including *Burkholderia* and *Yersinia*, 3-deoxy-D-*manno*-oct-2-ulosonic acid (Kdo) 3-hydroxylase, otherwise referred to as KdoO, converts Kdo to D-glycero-D-talo-oct-2-ulosonic acid (Ko) in an Fe(II)/α-ketoglutarate(α-KG)/O_2-dependent manner. This conversion renders the bacterial outer-membrane more stable and resistant to stresses such as an acidic environment. KdoO is a membrane-associated, deoxy-sugar hydroxylase that does not show significant sequence identity with any known enzymes and its structural information has not been previously reported. Here, we report the biochemical and

[*]To whom correspondence should be addressed: Hak Suk Chung: Center for Theragnosis, Biomedical Research Institute, Korea Institute of Science and Technology, Seoul 02792, Republic of Korea; hschung@kist.re.kr; Tel. +82-2-958-6423; Fax. +82-2-958-5919.

Accession numbers

The crystal structures have been deposited at the RCSB Protein Data Bank under the accession codes **6A2E** for $KdoO_{MI}$ (apoprotein), **5YKA** for $KdoO_{MI}$/Co(II), **5YVZ** for $KdoO_{MI}$/α-KG/Fe(III), and **5YW0** for $KdoO_{MI}$/succinate/Fe(III).

Author Contributions

H.S.C. expressed, purified protein and determined kinetic parameters. H.S.C. and C.W.P. crystallized, collected date, determined protein structures. H.S.C., C.W.P., and S.H.J. carried out refinement of the protein structures. H.S.C., S.H.J., and E.G.Y. wrote the manuscript. H.S.C., and C.R.H.R. designed and supervised the project.

Declaration of Interests

The authors declare no competing financial interests.

structural characterization of KdoO, Minf_1012 (Kdo_{MI}), from *Methylacidiphilum infernorum V4*. The *De novo* structure of Kdo_{MI} apoprotein indicates that $KdoO_{MI}$ consists of 13 α helices and 11 β strands, and has the jelly roll fold containing a metal binding motif, $HXDX_{111}H$. Structures of Kdo_{MI} bound to Co(II), Kdo_{MI} bound to α-KG and Fe(III), and Kdo_{MI} bound to succinate and Fe(III), in addition to mutagenesis analysis, indicate that His146, His260, and Asp148 play critical roles in Fe(II) binding, while Arg127, Arg162, Arg174, and Trp176 stabilize α-KG. It was also observed that His225 is adjacent to the active site and plays an important role in the catalysis of $KdoO_{MI}$ without affecting substrate binding, possibly being involved in oxygen activation. The crystal structure of $KdoO_{MI}$ is the first completed structure of a deoxy-sugar hydroxylase, and the data presented here have provided mechanistic insights into deoxy-sugar hydroxylase, KdoO and LPS biosynthesis.

Keywords

Kdo 3-hydroxylase (KdoO); x-ray structure; Fe(II)/α-ketoglutarate/O_2-dependent dioxygenase; lipopolysaccharide biosynthesis; deoxysugar oxidase

Introduction

Fe(II)/O_2/α-ketoglutarate (α-KG)-dependent dioxygenases are crucial for a variety of oxidative transformations in different biological pathways: the biosynthesis of antibiotics (kanamycin synthesis, fusicoccin and brassicicene syntheses, and A-90289 biosynthesis), morphine biosynthesis (T6ODM and CODM), DNA repair (AlkB), O_2-sensing in humans (HIF-hydroxylases and prolyl hydroxylase-2), histone demethylation (PHF8), and taurine catabolism (TauD) [1, 2]. The enzyme KdoO, 3-deoxy-D-*manno*-oct-2-ulosonic acid 3-hydroxylase, catalyzes the conversion of the outer Kdo unit of Kdo_2-lipid A to D-glycero-D-talo-oct-2-ulosonic acid (Ko) by replacing the axial hydrogen atom at the Kdo 3-position with OH (Figure 1A) [3]. Encouraged by the presence of the putative iron binding motif, $HXDX_{n>40}H$, we have demonstrated here that KdoO from *Burkholderia ambifaria AMMD* (*$KdoO_{BA}$*) and *Yersinia pestis* (*$KdoO_{YP}$*) is a Fe(II)/O_2/α-KG dependent dioxygenase (Figure 1). The enzyme is a membrane-associated protein that can be solubilized either by detergent or by high-salt-solution. It was determined that the His_6-tagged $KdoO_{BA}$ utilizes Kdo_2-lipid IV_A or Kdo_2-lipid A as substrates but does not use Kdo-lipid IV_A or heptosyl-Kdo_2-lipid A *in vitro*. Such substrate selectivity of KdoO indicates that KdoO functions after the Kdotransferase KdtA but prior to the heptosyl-transferase WaaC on the cytoplasmic surface of the inner membrane *in vivo* during Ko-containing lipopolysaccharide (LPS) biosynthesis (Figure S1). [4].

Homologues of KdoO are found exclusively in Gram-negative bacteria, including the human pathogens *Burkholderia mallei*, *Y. pestis*, *Klebsiella pneumoniae, Legionella longbeachae*, and *Coxiella burnetii*, as well as the plant pathogen *Ralstonia solanacearum*. It has been suggested that Ko formation in LPS increases the outer membrane stability of bacteria and may also modulate the binding of LPS to Toll-like receptor 4 and myeloid differentiation factor 2 of the mammalian innate immune system [3, 5]. Interestingly, KdoO is the first example of a sequenced deoxy-sugar hydroxylase, and its sequence identity with any known

proteins is not substantial enough to predict the structure of the KdoO enzyme. In this study, we identified, purified, and characterized KdoO from *Methylacidiphilum infernorum*. The crystal structures, including the apoenzyme and the cocrystals of $KdoO_{MI}$/Co(II), $KdoO_{MI}$/α-KG/Fe(III), and $KdoO_{MI}$/succinate/Fe(III), were solved for the first time. The structural information and site-directed mutagenesis identified the binding sites of Fe(II), α-KG, and succinate. In addition, we have found that His225 is adjacent to the active site and plays an important role in the catalysis of $KdoO_{MI}$ without affecting substrate binding, as it instead possibly involves in oxygen-molecule activation. Altogether, our data provide insights into the catalytic mechanism for the membrane-associated Fe(II)/O_2/α-KG-dependent dioxygenase, KdoO.

Results and Discussion

Minf_1012 is a homolog of KdoO in *M. infernorum V4*

M. infernorum V4 is an extremely acidophilic, methanotrophic, and aerobic bacterium isolated from soil and sediment at Hell's Gate, New Zealand, which grows optimally between pH 2.0 to 2.5 at 60 °C [6]. While the LPS structures of *M. infernorum* have not yet been reported, analysis of the *M. infernorum V4* genome using the Basic Local Alignment Search Tool (BLAST) [7] revealed Minf_1012 to be a homolog of Bamb_0774 ($KdoO_{BA}$) from *B. ambifaria* and Y1812 ($KdoO_{YP}$) from *Y. pestis*, (E values, 1e-86 and 8e-79, respectively). Minf_1012 shares 43.1% sequence identity with $KdoO_{BA}$ and 43.2% sequence identity with $KdoO_{YP}$ according to the ClustalW [8, 9] program, and it also contains a putative Fe(II) binding motif $HXDn_{>40}H$ (Figure 1B). All three KdoOs shown in Figure 1B have one HXD motif with three histidine residues that may be involved in binding to Fe(II). In order to determine if Minf_1012 functions as KdoO, we cloned *minf_1012* in pBAD33.1 [10] and transformed it into WBB06 [11], a heptosyl transferase-deficient mutant that synthesizes Kdo_2-lipid A as its only LPS. After growing strains in LB medium, we isolated LPS species through the Bligh-Dyer system [12] and analyzed them with thin-layer chromatography (TLC) as previously described [3, 4]. As shown in Figure 2A, the overexpression of Minf_1012 modified Kdo_2-lipid A to Ko-Kdo-lipid A. As the expression of Minf_1012 resulted in the conversion of Kdo_2-lipid A to Ko-Kdo-lipid A, we concluded that Minf_1012 is a Kdo 3-hydroxylase and renamed the gene and protein *$kdoO_{MI}$* and $KdoO_{MI}$, respectively.

Purification of $KdoO_{MI}$ and determination of specific activity

The His_6-tagged $KdoO_{MI}$ was overexpressed in *E. coli* C41(DE3) strain and purified to homogeneity as described in the methods section. $KdoO_{MI}$ protein was isolated in both cytosol and membrane fractions at about a 1:1.5 ratio in terms of total activity percentages (Table 1). Since the substrate Kdo_2-lipid A is located in the cytoplasmic side of the inner membrane, $KdoO_{MI}$ is expected to be a membrane-associated protein. $KdoO_{MI}$ was eluted as an aggregate in the absence of octyl α-D-glucopyranoside (OG), and the addition of OG (0.7%) yielded a homogenous protein from gel filtration chromatography. Compared to $KdoO_{BA}$, which was eluted as a monomeric protein from a gel filtration column without detergent [4], $KdoO_{MI}$ may have a more exposed hydrophobic surface. Following the chromatographic purification of $KdoO_{BA}$, the protein was analyzed by SDS PAGE (Figure

2B) and the specific activity was measured for each purification step (Table 1). The specific activity of $KdoO_{MI}$ increased about 34 times throughout the purification, and the purified protein showed more than 95% homogeneity. The specific activity of purified $KdoO_{MI}$ was measured at 120 ± 30 nmol/min/mg at 30 °C and the activity increased to 2900 ± 195 nmol/min/mg at 60 °C, the optimal temperature at which *M. infernorum* grows. The apparent K_m of purified $KdoO_{MI}$ with respect to Kdo_2-[4′−^{32}P]lipid A was 5.3 ± 1.2 μM, the apparent V_{max} was 362 ± 17 nmol min^{-1} mg^{-1} at 30 °C with 15 μM Fe(II) and 1 mM α-KG (Figure S2A), and the apparent K_d of $KdoO_{MI}$ with respect to Fe(II) was 5.3 ± 0.6 μM at 30 °C with 20 μM Kdo_2-[4′−^{32}P]lipid A and 1 mM α-KG (Figure S2B).

Structures of $KdoO_{MI}$: Apoprotein and Co(II) bound $KdoO_{MI}$

$KdoO_{MI}$ crystals were grown in one of two solutions: either in 0.1 M sodium acetate (pH=4.5), 200 mM lithium sulfate, and 50% v/v PEG400 or in 0.1 M sodium acetate (pH=4.6), 200 mM ammonium sulfate, and 25% v/v PEG4000. $KdoO_{MI}$ crystals belong to the space group $P2_12_12_1$ and diffracted to 1.45–1.94 Å (Table 2 and Table 3) using synchrotron radiation at the Southeast Regional Collaborative Access Team 22-BM beamline from the Advanced Photon Source, Argonne National Laboratory. The crystal structure of $KdoO_{MI}$/Co(II) was solved through the use of single-wavelength anomalous diffraction (SAD) phasing method based on the anomalous signal of a Co(II) ion in SHELX C/D/E [13]. All other structures were solved through molecular replacement [14] in PHENIX [15]. A search for similar structures in the Protein Data Bank (PDB) using the Dali database [16] revealed that the structure of human Egl nine homolog 1 (PHD2, PDB: 5LBB [17]), which hydroxylates Hypoxia-inducible factor [18] in an Fe(II)/α-KG/O_2-dependent manner, has the highest Z-score of 12.4. However, the sequence identities between PHD2 and $KdoO_{MI}$ are only a 7–8% match. Similar structures that were identified using the Dali database are all Fe(II)/α-KG/O_2-dependent dioxygenases that have less than 15% sequence identity with $KdoO_{MI}$.

Apoprotein $KdoO_{MI}$ crystal diffracted to 1.94 Å. We were able to determine the main-chain densities very well, with the exception of residues 67–69 (Loop 5 (L5) in Figure 3), possibly due to the higher degree of flexibility in this region. $KdoO_{MI}$ consists of 13 α helices and 11 β strands, and strands β5, β6, β7, β8, β9, β10, and β11 form a seven-stranded mixed β sheet that contains metal binding residues (Figure 3A, 3B, and 3C). This structure is similar to the jelly roll motif observed in the other Fe(II)/α-KG/O_2-dependent dioxygenase structures, often consisting of an eight-stranded mixed β sheet. Previous studies have indicated that $KdoO_{MI}$ should have a $HXDX_{n>40}H$ motif which is responsible for Fe(II) binding located in the jellyroll motif. The structure of the apoenzyme suggests that the His146, Asp148, and His260 in L11 and β10 are involved in Fe(II) binding (Figure 3B and 3C), and this was confirmed with the cocrystal structure of $KdoO_{MI}$/Co(II) (Figure 4).

In line with the two observations that 1) the purification of the monomeric enzyme requires detergent and 2) the enzyme utilizes Kdo_2-containing lipid A species, substrates that are located on the cytosolic face of the inner membrane, $KdoO_{MI}$ is expected to have a hydrophobic surface that interacts with the inner membrane. In order to obtain better information for the hydrophobic surface, the electrostatic surface of $KdoO_{MI}$ was calculated

using Adaptive Poisson-Boltzmann Software [19] (Figure 3D). According to these data, the residues from Phe202 through Thr210, which form a loop and are part of the α8 helix (Figure 3A and 3B), constitute a hydrophobic lobe. This lobe is located at the gate to the active site and is likely embedded in the inner membrane. Above the hydrophobic lobe and towards the active site, positively charged residues (Lys81, Arg139, Lys 140, Lys 144, Lys 200, Lys 211, Arg214, and Lys 227) form a surface (Figure 3D, Figure S3) that may interact with the negatively charged phosphate groups of phospholipids or two phosphate groups of the Kdo_2-lipid A species. These hydrophobic surfaces and positively charged residues might interact together with the bacterial inner membrane and the substrate. The superimposition of Apo $KdoO_{MI}$ and $KdoO_{MI}$/Co(II) complexes shows a 0.15 Å Root Mean Square Deviation (RMSD) in PyMOL [20] (Figure 4A), indicating that protein folding is complete before metal binding. The $KdoO_{MI}$/Co(II) structure further revealed that Co(II) has octahedral coordination: His146, Asp148, His260, and three water molecules complete the metal-coordination sphere (Figures 4B and 4C).

$KdoO_{MI}$/α-KG/Fe(III) complex structure and its implications.

In order to better understand the mechanism of $KdoO_{MI}$, we solved a structure for $KdoO_{MI}$/α-KG/Fe(III) complex at 1.6 Å resolution. According to this structure, Fe(III) is octahedrally coordinated by His146, Asp148, His260, an alpha-keto group and a carboxylic group from α-KG, and one water molecule (Figure 5A and 5B). α-KG was stabilized by electrostatic interactions with the positively charged residues within the jellyroll motif (Arg127, Arg162, and Arg174 located in β5, β6, and β7, respectively) as well as by a hydrogen bond with Trp176 located in β7 of $KdoO_{MI}$ (Figure 5C). Three arginine residues (Arg127, Arg162, and Arg174) form salt bridges with carboxylate groups of α-KG, presumably playing major roles in $KdoO_{MI}$ catalysis (Figure 5C). In order to examine the contributions of these four residues involved in α-KG stabilization, we constructed $KdoO_{MI}$ variants R127A, R162A, R174A, and W176A and determined their specific activities (Table 4). As expected, the R174A variant did not show any detectable activity (Table 4) while the R127A and R162A variants displayed 1.6% and 1.5% of the activity of the wild type $KdoO_{MI}$ enzyme, respectively. The W176A variant showed specific activity of about 40% of that of the wild type enzyme. Those critical residues involved in Fe(II) and α-KG binding are highly conserved among the KdoO homologues protein family, which sequences were aligned using COBALT program [21] (Figure S4).

As shown in Figure 1B, all KdoOs contain one HXD motif in their sequence whereas there are three histidine residues that possibly form the 2-His-1-Asp motif. Before obtaining $KdoO_{MI}$ structure, in order to pinpoint the last histidine residue, we conducted the site-directed mutagenesis study of $KdoO_{BA}$ with the conserved histidine residues of His213, His219, and His254. The catalytic activity of $KdoO_{BA}$ H219A and His254A variants are reduced to 6.9% and 7.16% of the wild type, respectively, whereas the activity in the $KdoO_{BA}$ H213A variant remains the same as in the wild type. Based on the $KdoO_{MI}$ structure, we now know that His254 in $KdoO_{BA,}$ corresponding to His260 in $KdoO_{MI}$ coordinates Fe(II) as a part of $HXDX_{n>40}H$ motif whereas the role of His219 $KdoO_{BA}$ is unclear. In the crystal structure of $KdoO_{MI}$/α-KG/Fe(III) complex, His225 in $KdoO_{MI}$, corresponding to His219 in $KdoO_{BA}$, is located in the helix α9, which is adjacent to the

metal binding sites (Figure 5D). In order to examine the contribution of His225 to the catalytic activity of $KdoO_{MI}$, we constructed a $KdoO_{MI}$ H225A variant and determined its specific activity (Table 4). As expected, the catalytic activity of $KdoO_{MI}$ H225A variant was 17.8% of the activity of the wild type protein. Initially, we speculated that His225 was involved in the binding of Kdo_2-lipid A substrate. In order to determine the contribution of His225 residue in substrate binding, we measured the apparent K_m values of Kdo_2-lipid A for $KdoO_{MI}$ wild type and $KdoO_{MI}$ H225A variant. Interestingly, the apparent K_m values were similar, at 4.0 ± 0.7 μM for $KdoO_{MI}$ H225A variant and 5.3 ± 1.2 μM for $KdoO_{MI}$ wild type. Even though H225A variation dramatically reduced specific activity, it did not change apparent K_m with respect to the substrate. This suggests that His225 is not involved in substrate binding. Unlike those residues involved in the binding of Fe(II) and α-KG, His225 is not absolutely conserved in KdoO homologues (Figure S4), as His225 is replaced with Arg242 in *Nitrosospira multiformis* KdoO, which shares ~ 32.0% and 31.5% sequence identity with $KdoO_{BA}$ and $KdoO_{MI}$, respectively (Figure S4). However, it has been suggested that both histidine and arginine residues stabilize the formations of superoxide in the catalytic mechanisms of catechol dioxygenase [22] and aminophenol cleavage dioxygenase [23]. Instead of substrate binding, His225 may be involved in the activation or stabilization of oxygen molecules, as it is about 6.4 Å and 5.3 Å apart from Fe(III) and iron-bound water, respectively (Figure 5D).

$KdoO_{MI}$/succinate/Fe(III) complex structure

The six coordination sites of Fe(III) were occupied by His146, Asp148, His260, a carboxylic acid unit of succinate, and two water molecules (Figure 6). In this structure, the terminal carboxylic acid unit of succinate forms salt bridges with Arg127 and Arg174 and a hydrogen bond with the Trp176 residue of $KdoO_{MI.}$ According to the structure, two salt bridges between one carboxylate of α-KG and the residues Arg162 and Arg127 found in the $KdoO_{MI}$/α-KG/Fe(III) structure were not observed. In addition, the succinate only occupied one coordination site of Fe(III) in the $KdoO_{MI}$/succinate/Fe(III) complex. These reduced interactions between succinate with $KdoO_{MI}$/Fe(III) may allow for the next catalytic cycle by replacing succinate with α-KG.

In conclusion, KdoO is a non-heme dioxygenase and a membrane-associated protein that acts upon the biologically significant Kdo_2-containing lipid A species. It converts this species to Ko-Kdo containing lipid A species during LPS biosynthesis. This modification increases the stability of the glycosidic bond between Ko-Kdo and lipid A while also strengthening the Ko and Kdo bond, which possibly destabilizes the oxonium ion, the intermediate of acidic hydrolysis, resulting in resistance to acidic environments [3]. Considering that *M. infernorum* lives in acidic conditions with high temperatures, a Ko-Kdolipid A structure may be beneficial for the bacterium. In this study, we defined the function and kinetic parameters of $KdoO_{MI}$ and determined high resolution *de novo* structures of $KdoO_{MI}$ apoenzyme, $KdoO_{MI}$/Co(II), $KdoO_{MI}$/α-KG/Fe(III), and Kdo_{MI}/succinate/Fe(III) structures. These are the first reported structures of proteins from the KdoO enzyme family determined by x-ray crystallography. We identified His146, Asp148, and His260 as Fe(II) binding residues, and Arg127, Arg162, Arg174, and Trp176 as α-KG binding residues through the use of structural information and mutational analysis. Finally,

we identified that His225 plays a significant role in catalysis and is possibly involved in oxygen-molecule activation. Further studies are required to better understand how KdoO recognizes the substrate and an oxygen molecule.

Materials and methods

Materials.

Chloroform, methanol, and silica gel 60 (0.25 mm) thin layer chromatography plates, as well as high-performance analytical thin layer chromatography plates were purchased from EMD Chemicals Inc. (Gibbstown, NJ). Tryptone, yeast extract, and agar were purchased from Becton, Dickinson and Co. (Franklin Lakes, NJ). Isopropyl 1-thio-β-D-galactopyranoside (IPTG) was purchased from Invitrogen Corp. (Carlsbad, CA). [$\gamma-^{32}$P]ATP (3 mCi/nmol) and Phosphophorous-32 were from PerkinElmer Life and Analytical Sciences Inc. (Waltham, MA). All other chemicals, including α-KG, $FeCl_3$ and $Fe(NH_4)_2(SO_4)_2$, were reagent grade and were purchased from either Sigma-Aldrich or Mallinckrodt Baker Inc. (Phillipsburg, NJ). Purified Kdo_2-lipid A was obtained from Avanti Polar Lipids Inc. (Alabaster, AL).

Bacterial strains.

pBAD33.1/WBB06 and pMiKdoO/WBB06 were constructed by transformation of pBAD33.1 and pMiKdoO into *E. coli* WBB06. pET21b-$KdoO_{MI}$/C41(DE3) was constructed by transformation of pET21b-$KdoO_{MI}$ into *E. coli* C41(DE3). Typically, bacteria were grown in LB medium, which contains 10 g of tryptone, 5 g of yeast extract and 10 g of NaCl per liter [24]. For the selection of plasmids, cells were grown in the presence of 50 μg/mL ampicillin (Amp), 30 μg/mL chloramphenicol, 0.2% L-arabinose (L-Ara), and/or 1 mM IPTG.

Molecular biology techniques.

Protocols for the handling of DNA and the preparation of *E. coli* cells for electroporation derived from Sambrook and Russell [25]. Chemical transformation-competent *E. coli* cells were prepared by the method of Inoue *et al.* [26]. Plasmids were isolated from cell cultures using the QIAprep Miniprep kit. T4 DNA ligase, restriction endonucleases, and calf intestinal alkaline phosphatase (CIP) were purchased from New England Biolabs (Ipswich, MA) and used according to the manufacturers' instructions. Double-stranded DNA sequencing was performed with an ABI Prism 377 instrument at the Duke University DNA Analysis Facility or at Eton Biosceince INC (Durham, NC). Primers came from IDT Inc. (Coralville, IA).

Plasmid constructions and transformations into *E. coli* C41(DE3) and WBB06

The encoding DNA sequence for $KdoO_{MI}$ (Minf_1012, see also Figure S5) was synthesized by IDT Inc. (Coralville, IA) and amplified with primers, NdeI-$kdoO_{MI}$-5 (5'-GGCGCAGCATATGTTCCCGATGGACACCAAAAC-3') and HindIII-stop-$kdoO_{MI}$-3 (5'-GCAGAAGCTTTCAGAACGATTCAGATGACAC CAGTTT TTTATTCA −3') for pMiKdoO and NdeI-$kdoO_{MI}$-5 and HindIII-$kdoO_{MI}$-3 (5'-GCAGAAGCTTGAACGATTCAGATGACACCAGTTTTTTATTCA −3') for pET21b-

$KdoO_{MI}$. Amplified DNA was digested with NdeI and HindIII. The resulting PCR fragments were ligated into pBAD33.1 or pET21b, which were digested with the same enzymes and treated with CIP. The resulting plasmids were named, “pMiKdoO” and “pET21b-$KdoO_{MI}$”.All alanine variants were generated by the Quikchange PCR protocol provided by Stratagene, using pET21b-$KdoO_{MI}$ as the template in conjunction with the following primers: prR127A-5 (5’-TGCTCGTACGAGCTTCGCCCCGGTTGAAAT CAGT-3’) and prR127A-3 (5’-ACTGATTTCAACCGGGGCGAAGCTCGTACGAGCA-3’), prR162A-5 (5’-CGGTGAACGTATTCTGGCCGTCTTCAGCAACATC-3’) and prR162A-3 (5’-GATGTTGCTGAAGACGGCCAGAATACGTTCACCG-3’), prR174A-5 (5’-TCCGCAGGGCAAACCGGCGTCTTGGCGCATTGGTG-3’) and prR174A-3 (5’-CACCAATGCGCCAAGACGCCGGTTTGCCCTGCGGA-3’), prW176A-5 (5’-GGGCAAACCGCGTTCTGCGCGCATTGGTGAACC-3’) and prW176A-3 (5’-GGTTCACCAATGCGCGCAGAACGCGGTTTGCCC-3’), and prH225A-5 (5’-ATTACATGCTGGAACTGGCCGATAAAGGTAAACT-3’) and prH225A-3 (5’-AGTTTACCTTTATCGGCCAGTTCCAGCATGTAAT-3’) for pR127A, pR162A, pR174A, pW176A, and pH225A, respectively. H213A $KdoO_{BA}$, H219A $KdoO_{BA}$, H254A $KdoO_{BA}$ were made by Quikchange PCR with the primers prHSC196 (5’-CAGCGCGTACGACGCCCTGATGCTGAACCT-3’) and prHSC197 (5’-AGGTTCAGCATCAGGGCGTCGTACGCGCTG-3’) for H213A $KdoO_{BA}$, prHSC198 (5’-TGATGCTGAACCTGGCCGACGGGATGAAGGC-3’) and prHSC199 (5’-GCCTTCATCCCGTCGGCCAGGTTCAGCATCA-3’) for H219A $KdoO_{BA}$, and prHSC200 (5’- CGGATCAGACTTCGGCCGCTGTGATGTCCGG-3’) and prHSC201 (5’-CCGGACATCACAGCGGCCGAAGTCTGATCCG-3’) for H254A $KdoO_{BA}$, and $pKdoO_{BA}$.3 [4] as the template. The resulting plasmids were all confirmed by sequencing using the primers T7F and T7R and transformed into C41(DE3) [27].

Growth and lipid extraction of WBB06/pBAD33.1 and WBB06/pMiKdoO.

Cells were grown overnight in LB medium supplemented with 30 μg/mL of chloramphenicol. 1 mL of the overnight culture was inoculated in 100 mL LB medium, which contained 0.2% L-Ara and 30 μg/mL of chloramphenicol at 37 °C, and was shaken at 200 rpm. Cells were harvested when OD_{600}~ 1.0 and the pellets were washed with 20 mL of PBS; lipid was extracted through the Bligh-Dyer system described previously [3, 4, 12]

To analyze the lipids, thin-layer chromatography was executed as previously described [3, 4]

Purification of $KdoO_{MI}$-His_6.

C41(DE3)/pET21b-$KdoO_{MI}$ was grown in 3 L LB media containing 50 μg/mL of ampicillin at 37 °C to an OD_{600} ~ 0.25. Next, the cell cultures were cooled to 18 °C, induced with 1 mM IPTG at OD_{600} ~ 0.6, and grown for 15–18 hours at 18 °C (OD_{600} ~ 4.5). The cells were then harvested and washed with phosphate-buffered saline [28]. They were re-suspended in 80 mL of 50 mM 4-(2-hydroxyethyl)-1-piperazineethanesulfonic acid (HEPES) (pH=7.5) and supplemented with 100 mM sodium chloride. Cells were lysed by passage through a French pressure cell at 17,000 psi, and the lysate was centrifuged at 8,000 *x g* to remove cell debris. A portion of the supernatant was retained as the “cell-free lysate.” Cell-free lysate from $KdoO_{MI}$-His_6 was centrifuged at 45,000 rpm (~140,000 *x g*) in a

Beckman 70.1 Ti rotor for 1 h at 4 °C. The supernatant was the “membrane-free lysate.” The membrane pellet was re-suspended and homogenized in 10 mL and then immediately diluted to 62 mL of 50 mM HEPES (pH=7.5), 100 mM NaCl, and 2 mM EDTA. The resulting solution was centrifuged at 45,000 rpm (~140,000 *x g*) in a Beckman 70.1 Ti rotor for 1 h at 4 °C. The supernatant was the “EDTA wash” fraction. The membrane pellet was re-suspended and homogenized in 12.5 mL and diluted to 95 mL of 50 mM HEPES (pH=7.5), 300 mM NaCl, 20% glycerol (buffer A), and 1.5% Triton X-100. This solution was incubated and gently shaken for 90 minutes at 4 °C. The solution was again centrifuged at 40,000 rpm (~110,000 *x g*) in a Beckman 50.2 rotor for 1 h at 4 °C. The supernatants were retained as the “solubilized membrane fraction (95 mL),” and the pellet was re-suspended and homogenized in 12.8 mL of 1.5% Triton X-100 in buffer A to yield the “insoluble membrane fraction.” The solubilized membrane fraction (94 mL) was incubated with 8 mL pre-washed Ni-nitrilotriacetic acid (**NTA**) resin for 60 minutes and was gently exposed to inversion mixing at 4 °C in the presence of 20 mM imidazole. The solute was packed into a column and then washed with 80 mL of 0.1% triton X-100 and 20 mM imidazole in buffer A. The Ni-NTA resin was subsequently washed with 220 mL of 20 mM and 230 mL of 50 mM imidazole in buffer A at 4 °C. $KdoO_{MI}$-His_6 was eluted with one fraction of 10 mL, three 45mL fractions of 300 mM imidazole in buffer A. Each elution fraction was immediately supplemented with 0.5 M EDTA (pH=7.5), to yield a final concentration of 2 mM EDTA, and was kept at 4 °C. Fractions containing $KdoO_{MI}$-His_6 were visualized by SDS-PAGE and concentrated to a final volume of 10.5 mL with 0.7% OG at 4 °C. Next, the sample was passed through a 0.2 μm filter (Millipore, Billercia, MA), and 9.0 mL of sample was loaded onto a 320 mL calibrated size-exclusion column (Superdex 200 XK26/70; GE Healthcare, Waukesha, WI), equilibrated with buffer A containing 0.7% OG and 1 mM EDTA at 4 °C. The sample was passed through at a rate of 1.25 mL/min using an AKTA FPLC system equipped with the UNICORN program (GE Healthcare, Waukesha, WI) at 4 °C. Elution with 1.1 column volumes (350 mL) was at 1 mL/min, and 5 mL fractions were collected. Fractions containing $KdoO_{MI}$-His_6, as judged by A_{280} and SDS-PAGE, were pooled and concentrated to 8 mg/mL using Amicon Ultra 10000 molecular weight cutoff centrifugal concentration devices (Millipore, Billercia, MA) at 4 °C. Concentrated samples were dialyzed against buffer containing 25 mM HEPES (pH 7.5), 0.2 M NaCl, 20% glycerol, 0.7% OG, and 2 mM EDTA for 20 hours at 4 °C. Protein was diluted to 7–8 mg/mL and stored at −80 °C. Protein concentrations were determined by the bicinchoninic acid assay or Bradford assay (Thermo Fisher Scientific, Rockford, IL) with bovine serum albumin (BSA) as standard [29]. The results are summarized in Table 1 and Figure 2B.

Purification of $KdoO_{MI}$-His_6 variants.

Variants were purified by Ni-NTA affinity column chromatography as described for $KdoO_{MI}$-His_6 and then EDTA and OG were added to yield final concentrations of 1 mM and 0.7%, respectively.

Purification of $KdoO_{BA}$-His_6 wild type and variants.

$KdoO_{BA}$ H213A, $KdoO_{BA}$ H219A, and $KdoO_{BA}$ H254A variants were purified by Ni-NTA affinity column chromatography as described for $KdoO_{BA}$ [4].

Preparation of Kdo_2-lipid A.

Kdo_2-lipid A was purchased from Avanti Polar Lipids. Inc (Alabaster, USA)

Preparation of radiolabeled substrates.

^{32}P-labeled Kdo_2-lipid A substrate was prepared according to the published procedures in reference [4].

In vitro Assay of $KdoO_{MI}$-His_6.

In vitro assay for purified $KdoO_{MI}$-His_6 was executed following the previously described method [3, 4] with modifications. The reaction mixture (typically in a final volume of 20 μL) contained 50 mM HEPES (pH=7.5), 1 mM α-KG, 2 mM ascorbate, 15 μM $Fe(NH_4)_2(SO_4)_2$, 0.1% Triton X-100, 0.5 mg/mL BSA, and 5 μM Kdo_2-[4'−^{32}P]lipid A (~300,000 cpm/nmol). Ascorbate, α-KG, and $Fe(NH_4)_2(SO_4)_2$ solutions were freshly prepared before each assay using H_2O de-gassed with N_2 (g). Just before assaying, $KdoO_{MI}$-His_6 from stock solution (1–5 mg/mL) was diluted with a buffer containing 50 mM HEPES (pH=7.5), 100 mM NaCl, and 0.5 mg/mL of BSA. Assays were carried out at 30 °C. Reactions were initiated by adding $KdoO_{MI}$-His_6 and terminated by spotting 1.5–2 μL of the reaction mixtures onto the origin of a 20 × 20 cm Silica Gel 60 TLC plate. The plate was dried with a cold air stream and the lipids were separated by TLC in the freshly prepared and equilibrated tank containing the solvent chloroform:methanol:acetic acid:H_2O (25:15:3.5:4, v/v). Following chromatography, the TLC plate was dried under a hot air stream and was exposed to a PhosphorImager screen for 12–16 h. The extent of conversion of Kdo_2- [4'−^{32}P]lipid A to Ko-Kdo-[4'−^{32}P]lipid A was determined with a PhosphorImager (GE Healthcare), equipped with ImageQuant software. To measure relative activities of variants and wild type $KdoO_{MI}$, the enzyme reactions were carried out in 20 μL solution containing 50 mM HEPES (pH=7.5), 0.5 mM α-KG, 2 mM ascorbate, 60 μM $Fe(NH_4)_2(SO_4)_2$, 0.1% Triton X-100, 0.5 mg/mL BSA, and 20 μM Kdo_2-[4'−^{32}P]lipid A (~300,000 cpm/nmol).

Kinetic Parameters of $KdoO_{MI}$.

To determine the K_m and V_{max} of $KdoO_{MI}$-His_6 with respect to 0–200 μM

Kdo_2-lipid A, the purified enzyme was assayed as described above. The concentration of $KdoO_{MI}$ in the assay was varied from 0.1 to 6 μg/mL to maintain linear conversion to product with time at different Kdo_2-lipid A concentrations. To determine apparent K_d of Fe(II), the activities of $KdoO_{MI}$ were measured in the presence of 1.5–100 μM of Fe(II), 20 μM of Kdo - [4'−^{32}P]lipid A, 0.5 mM α-KG, and 3 μg/mL of $KdoO_{MI}$-His_6. KaleidaGraph was used to fit velocities to the Michaelis−Menten equation [30].

Crystallization and structure determination.

Crystals of $KdoO_{MI}$ were grown within 30 days by using a sitting drop vapor diffusion method in drops containing 4 to 6 or 5 to 5 proportional volumes of protein solution (7.2 mg/mL) and reservoir solution (0.1 M sodium acetate (pH 4.5), 160–240 mM lithium sulfate, 50% v/v PEG400) or reservoir solution (0.1 M sodium acetate (pH 4.6), 160–240 mM ammonium sulfate, 25% v/v PEG4000) at 15 °C or 20 °C, respectively. Crystals were

soaked for about 1–12 hours in 25 mM HEPES (pH 7.2), 15 mM NaCl, 1 mM EDTA, 10% glycerol, 2 mM Co(II) or Fe(III), 50 mM $LiSO_4$, 5 mM α-KG or 5 mM succinate, and 60% PEG400, and were immediately flash-frozen in liquid nitrogen. Data were collected at the Co(II) absorption peak (1.5 Å) and data sets for other crystals were obtained at the wavelength 1.0 Å on the Southeast Regional Collaborative Access Team (SER-CAT) BM-22 line at the Advanced Photon Source (APS, Argonne National Laboratory). A Co(II) SAD dataset with 1.9 Å resolution was obtained. The data set was reduced and scaled using HKL-2000 [31]. Identification of heavy-atom sites, calculating phases using SHELX C/D/E [13], and initial model building was done using Autobuild within the PHENIX [15]. Model building and refinements were done using COOT [32] and PHENIX [15]. Phases for apoprotein and other complexes were determined through molecular replacement using the model from$KdoO_{MI}$/Co(II) structure in PHENIX [15]. The final model was validated via MOLPROBITY [33]. The statistics are summarized in Table 2 and 3.

Supplementary Material

Refer to Web version on PubMed Central for supplementary material.

Acknowledgements

We thank Arman Kassam and Dr. Ali Masoudi for their critical reading of the manuscript. Crystallization, screening, data collection, and data processing were performed at the Duke University X-ray Crystallography Shared Resource Center. Diffraction data were collected at the Southeast Regional Collaborative Access Team 22-BM beamline at the Advanced Photon Source, Argonne National Laboratory; use of the Advanced Photon Source was supported by the US Department of Energy, Office of Science, and the Office of Basic Energy Sciences under contract W-31–109-Eng-38. This research was funded by the National Institutes of Health Grant GM-51310 (to C.R.H.R.), by the Pioneer Research Center Program (2014M3C1A3054141) through the National Research Foundation of Korea funded by the Ministry of Science, ICT & Future Planning, by National Research Foundation of Korea (NRF) Grants (No. 2018R1A2B2008995) and by the Intramural Research Program of KIST.

Abbreviations

α-KG	alpha-ketoglutarate
$KdoO_{MI}$	*Methylacidiphilum infernorum* KdoO
$KdoO_{BA}$	*Burkholderia ambifaria* KdoO
$KdoO_{YP}$	*Yersinia pestis* KdoO
BCA	bicinchoninic acid
FPLC	fastprotein liquid chromatography
HEPES	4-(2-hydroxyethyl)-1-piperazineethanesulfonic acid
IPTG	1-thiogalactopyranoside
Kdo	3-deoxy-D-manno-oct-2-ulosonic acid
KdoO	Kdo hydroxylase
Ko	D-glycero-D-talo-oct-2-ulosonic acid

LPS	lipopolysaccharide
PAGE	polyacrylamide gel electrophoresis
PBS	phosphate-buffered saline
TLC	thin layer chromatography

References

[1]. Islam MS, Leissing TM, Chowdhury R, Hopkinson RJ, Schofield CJ. 2-Oxoglutarate-Dependent Oxygenases. Annu Rev Biochem. 2018;87:585–620. [PubMed: 29494239]

[2]. Martinez S, Hausinger RP. Catalytic Mechanisms of Fe(II)- and 2-Oxoglutarate-dependent Oxygenases. J Biol Chem. 2015;290:20702–11. [PubMed: 26152721]

[3]. Chung HS, Raetz CR. Dioxygenases in Burkholderia ambifaria and Yersinia pestis that hydroxylate the outer Kdo unit of lipopolysaccharide. Proc Natl Acad Sci U S A. 2011;108:510–5. [PubMed: 21178073]

[4]. Chung HS, Yang EG, Hwang D, Lee JE, Guan Z, Raetz CR. Kdo hydroxylase is an inner core assembly enzyme in the Ko-containing lipopolysaccharide biosynthesis. Biochem Biophys Res Commun. 2014;452:789–94. [PubMed: 25204504]

[5]. Park BS, Song DH, Kim HM, Choi BS, Lee H, Lee JO. The structural basis of lipopolysaccharide recognition by the TLR4-MD-2 complex. Nature. 2009;458:1191–5. [PubMed: 19252480]

[6]. Dunfield PF, Yuryev A, Senin P, Smirnova AV, Stott MB, Hou S, et al. Methane oxidation by an extremely acidophilic bacterium of the phylum Verrucomicrobia. Nature. 2007;450:879–82. [PubMed: 18004300]

[7]. Altschul SF, Madden TL, Schaffer AA, Zhang J, Zhang Z, Miller W, et al. Gapped BLAST and PSI-BLAST: a new generation of protein database search programs. Nucleic Acids Res. 1997;25:3389–402. [PubMed: 9254694]

[8]. Thompson JD, Higgins DG, Gibson TJ. CLUSTAL W: improving the sensitivity of progressive multiple sequence alignment through sequence weighting, position-specific gap penalties and weight matrix choice. Nucleic Acids Res. 1994;22:4673–80. [PubMed: 7984417]

[9]. Combet C, Blanchet C, Geourjon C, Deleage G. NPS@: network protein sequence analysis. Trends Biochem Sci. 2000;25:147–50. [PubMed: 10694887]

[10]. Chung HS, Raetz CR. Interchangeable domains in the Kdo transferases of Escherichia coli and Haemophilus influenzae. Biochemistry. 2010;49:4126–37. [PubMed: 20394418]

[11]. Brabetz W, Muller-Loennies S, Holst O, Brade H. Deletion of the heptosyltransferase genes rfaC and rfaF in Escherichia coli K-12 results in an Re-type lipopolysaccharide with a high degree of 2-aminoethanol phosphate substitution. Eur J Biochem. 1997;247:716–24. [PubMed: 9266718]

[12]. Bligh EG, Dyer WJ. A rapid method of total lipid extraction and purification. Can J Biochem Physiol. 1959;37:911–7. [PubMed: 13671378]

[13]. Sheldrick GM. Experimental phasing with SHELXC/D/E: combining chain tracing with density modification. Acta Crystallogr D. 2010;66:479–85. [PubMed: 20383001]

[14]. McCoy AJ, Grosse-Kunstleve RW, Adams PD, Winn MD, Storoni LC, Read RJ. Phaser crystallographic software. J Appl Crystallogr. 2007;40:658–74. [PubMed: 19461840]

[15]. Adams PD, Afonine PV, Bunkoczi G, Chen VB, Davis IW, Echols N, et al. PHENIX: a comprehensive Python-based system for macromolecular structure solution. Acta Crystallogr D. 2010;66:213–21. [PubMed: 20124702]

[16]. Holm L, Rosenstrom P. Dali server: conservation mapping in 3D. Nucleic Acids Res. 2010;38:W545–9. [PubMed: 20457744]

[17]. Chowdhury R, Leung IKH, Tian YM, Abboud MI, Ge W, Domene C, et al. Structural basis for oxygen degradation domain selectivity of the HIF prolyl hydroxylases. Nat Commun. 2016;7.

[18]. Epstein ACR, Gleadle JM, McNeill LA, Hewitson KS, O'Rourke J, Mole DR, et al. C-elegans EGL-9 and mammalian homologs define a family of dioxygenases that regulate HIF by prolyl hydroxylation. Cell. 2001;107:43–54. [PubMed: 11595184]

[19]. Baker NA, Sept D, Joseph S, Holst MJ, McCammon JA. Electrostatics of nanosystems: application to microtubules and the ribosome. Proc Natl Acad Sci U S A. 2001;98:10037–41. [PubMed: 11517324]

[20]. Schrodinger LLC. The PyMOL Molecular Graphics System, Version 1.8. 2015.

[21]. Papadopoulos JS, Agarwala R. COBALT: constraint-based alignment tool for multiple protein sequences. Bioinformatics. 2007;23:1073–9. [PubMed: 17332019]

[22]. Mendel S, Arndt A, Bugg TD. Acid-base catalysis in the extradiol catechol dioxygenase reaction mechanism: site-directed mutagenesis of His-115 and His-179 in Escherichia coli 2,3-dihydroxyphenylpropionate 1,2-dioxygenase (MhpB). Biochemistry. 2004;43:13390–6. [PubMed: 15491145]

[23]. Zhang Y, Colabroy KL, Begley TP, Ealick SE. Structural studies on 3-hydroxyanthranilate-3,4-dioxygenase: the catalytic mechanism of a complex oxidation involved in NAD biosynthesis. Biochemistry. 2005;44:7632–43. [PubMed: 15909978]

[24]. Miller JR. Experiments in Molecular Genetics.: Cold Spring Harbor, NY: Cold Spring Harbor Laboratory;; 1972.

[25]. Sambrook JG, Russell DW. Molecular Cloning: A Laboratory Manual.: Cold Spring Harbor, NY: Cold Spring Harbor Laboratory;; 2001.

[26]. Inoue H, Nojima H, Okayama H. High efficiency transformation of Escherichia coli with plasmids. Gene. 1990;96:23–8. [PubMed: 2265755]

[27]. Miroux B, Walker JE. Over-production of proteins in Escherichia coli: mutant hosts that allow synthesis of some membrane proteins and globular proteins at high levels. J Mol Biol. 1996;260:289–98. [PubMed: 8757792]

[28]. Dulbecco R, Vogt M. Plaque formation and isolation of pure lines with poliomyelitis viruses. J Exp Med. 1954;99:167–82. [PubMed: 13130792]

[29]. Smith PK, Krohn RI, Hermanson GT, Mallia AK, Gartner FH, Provenzano MD, et al. Measurement of Protein Using Bicinchoninic Acid. Analytical Biochemistry. 1985;150:76–85. [PubMed: 3843705]

[30]. Bartling CM, Raetz CR. Steady-state kinetics and mechanism of LpxD, the N-acyltransferase of lipid A biosynthesis. Biochemistry. 2008;47:5290–302. [PubMed: 18422345]

[31]. Otwinowski Z, Minor W. Processing of X-ray diffraction data collected in oscillation mode. Method Enzymol. 1997;276:307–26.

[32]. Emsley P, Cowtan K. Coot: model-building tools for molecular graphics. Acta Crystallogr D. 2004;60:2126–32. [PubMed: 15572765]

[33]. Chen VB, Arendall WB, Headd JJ, Keedy DA, Immormino RM, Kapral GJ, et al. MolProbity: all-atom structure validation for macromolecular crystallography. Acta Crystallogr D. 2010;66:12–21. [PubMed: 20057044]

Highlights

- KdoO converts Kdo to Ko during LPS biosynthesis.
- Minf_1012 from *Methylacidiphilum infernorum* functions as $KdoO_{MI}$.
- The first completed structures of $KdoO_{MI}$ are determined at 1.45–1.94 Å resolution.
- The structure of $KdoO_{MI}$ reveals a metal binding motif $HXDX_{N>40}H$.
- Cosubstrate bound $KdoO_{MI}$ and mutagenesis study show important residues for catalysis.

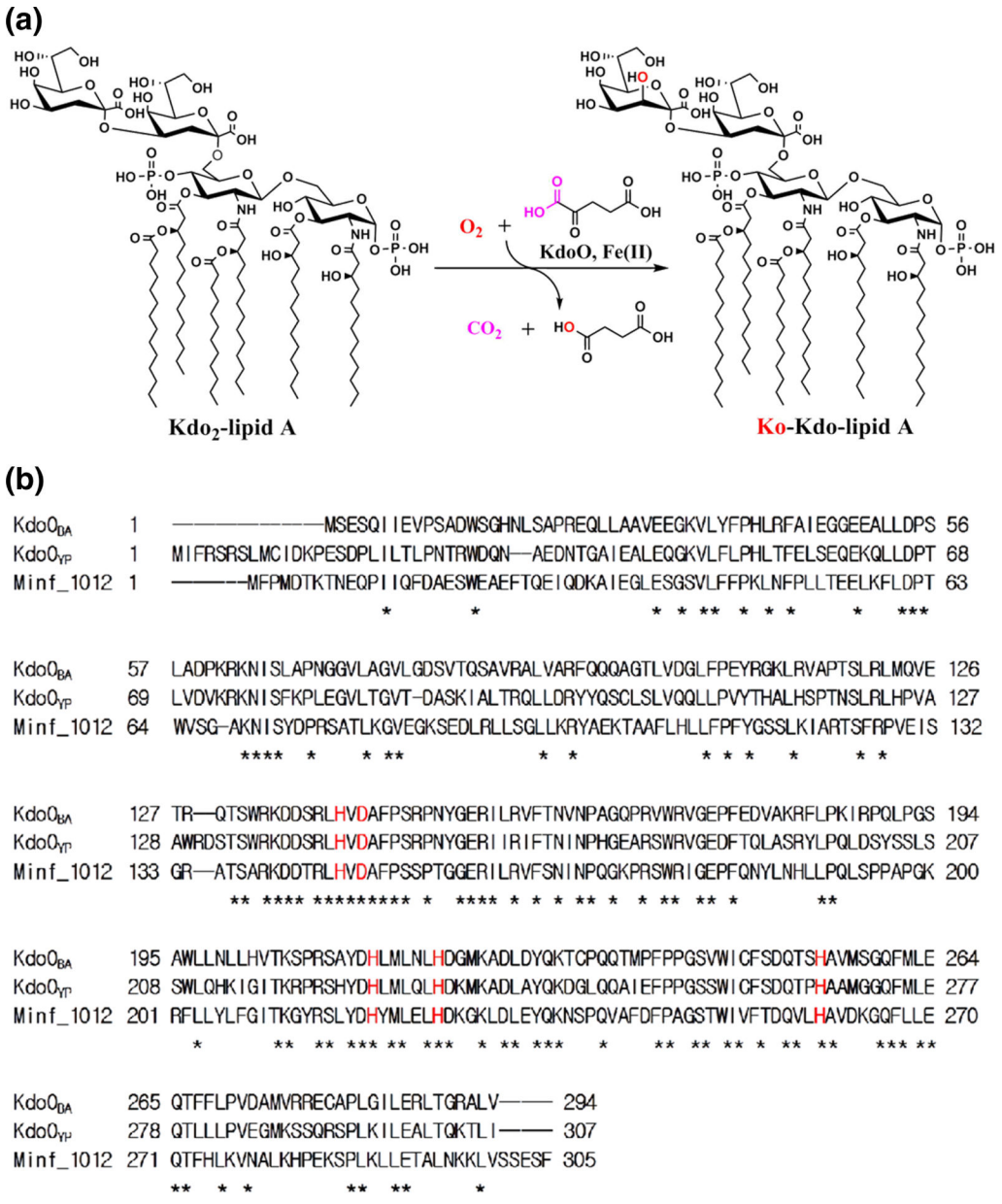

Figure 1.

A KdoO homologue in *M. infernorum V4*. (A) KdoO converts Kdo_2-lipid A to Ko-Kdo-lipid A in a Fe(II)/O_2/α-KG dependent manner during LPS biosynthesis of *B. ambifaria* and *Y. pestis*. (B) Sequence alignment of $KdoO_{BA}$ from *B. ambifaria*, $KdoO_{YP}$ from *Y. pestis*, and Minf_1012 from *M. infernorum V4*. The three proteins share 34.29% identity (designated by asterisk) and 49.53% similarity. These proteins contain the potential iron-binding motif, HXDXnH (n> 40, there are three potential downstream His residues) shown in red. Minf_1012 shares 43.1% sequence identity with $KdoO_{BA}$ and 43.2% sequence identity with $KdoO_{YP}$ according to the ClustalW [8, 9].

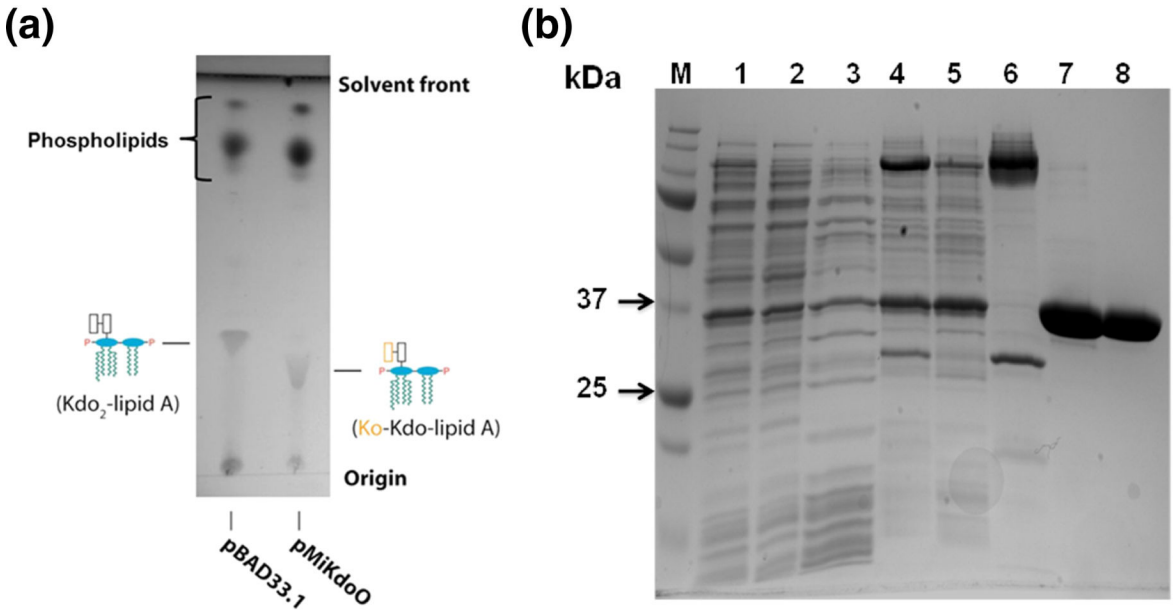

Figure 2.

Ko-Kdo-lipid A formation by Minf_1012 and purification and characterization of the enzyme. (A) TLC plates of Lipid A species extracted from WBB06 carrying pBAD33.1 or pMiKdoO. The TLC plates were developed in chloroform:methanol:acetic acid:H_2O (25:15:3.5:4 v/v) and visualized through a charring method. (B) SDS−PAGE analysis of protein from each step of the $KdoO_{MI}$ purification. Approximately 15 μg of protein were loaded in each lane. Descriptions follow the numbers in Table 1.

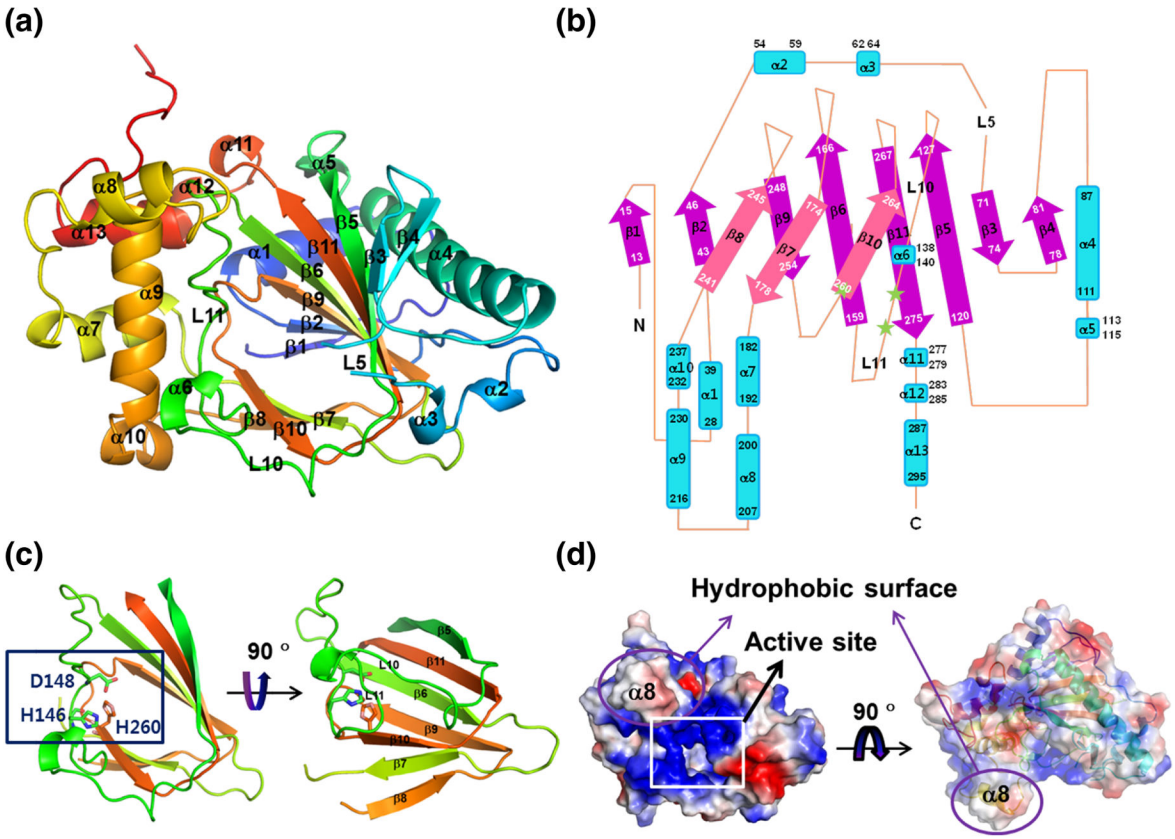

Figure 3.

Structure of $KdoO_{MI}$ apoprotein. (A) Cartoon diagram of $KdoO_{MI}$. (B) Topology of $KdoO_{MI}$. Green stars represent His146, Asp148, and His260. (C) Jellyroll-like structure containing His146, Asp148, and His260 of $KdoO_{MI}$ apoprotein. (D) The electrostatic surface of $KdoO_{Mi}$ as calculated by the Adaptive Poisson-Boltzmann Solver [19]. The electrostatic potential is scaled from −3.0 (red) to +3.0 (blue) kT/e. Figures were rendered using PyMOL [20].

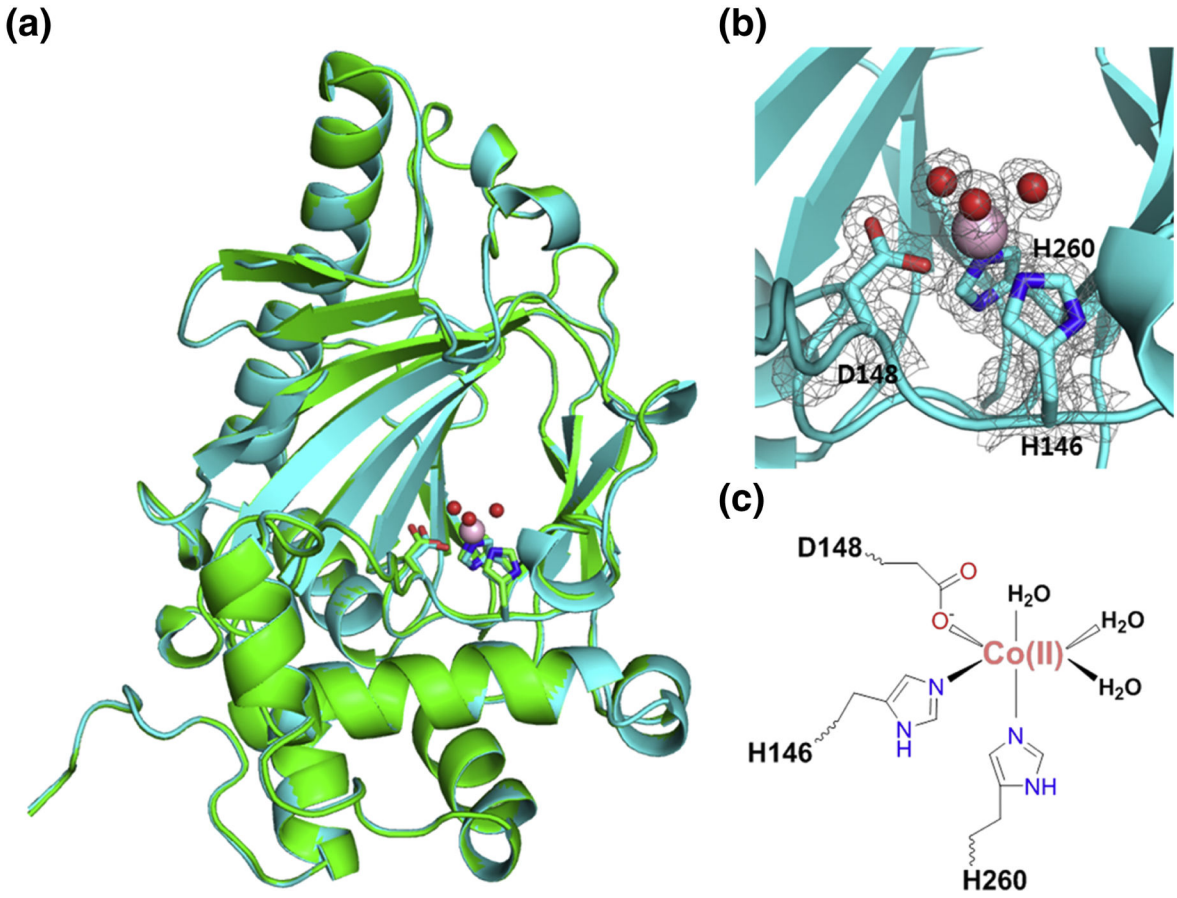

Figure 4.

$KdoO_{MI}$/Co(II) complex structure. (A) The globally aligned cartoon illustrations of apoprotein (green) and $KdoO_{MI}$/Co(II) complex (blue). (B) Co(II) (deepsalmon) bound $KdoO_{MI}$ (blue). Three water molecules coordinate Co(II) shown in red non-bound spheres. Corresponding simulated annealing omit electron density (gray mesh) for His146, Asp148, His260, Co(II), and three water molecules was calculated with coefficients $2\mathbf{F}_o - \mathbf{F}_c$, contoured at 1 σ. (C) Schematic overview of the Co(II) binding site.

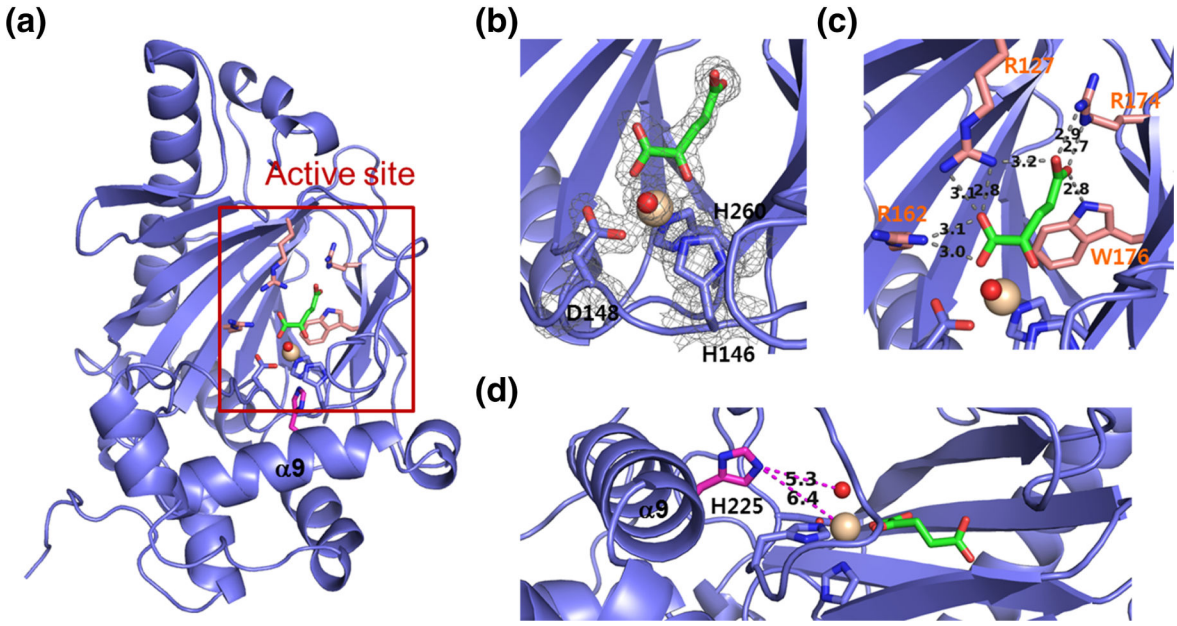

Figure 5.

Residues Arg127, Arg162, Arg174, and Trp176 involved in α-KG binding in $KdoO_{MI}$/α-KG/Fe(III) complex (slate). (A) Fe(III) and α-KG bound $KdoO_{MI.}$ (B) Corresponding simulated annealing omit electron density (gray mesh) for His146, Asp148, His260, Fe(III), water, and α-KG was calculated with coefficients $2\mathbf{F}_o - \mathbf{F}_c$, contoured at 1 σ. (C) Close-up of the Fe(III)/α-KG binding site. Salt bridges and hydrogen bonds between α-KG and $KdoO_{MI}$ are indicated with dashed lines, along with their distances. (D) Close-up of His225 and the active site of $KdoO_{MI}$. Fe(III) (wheat sphere), α-KG (green stick), water (red non-bonded sphere), and His225 (magenta stick) in $KdoO_{MI}$/α-KG/Fe(III) complex are shown.

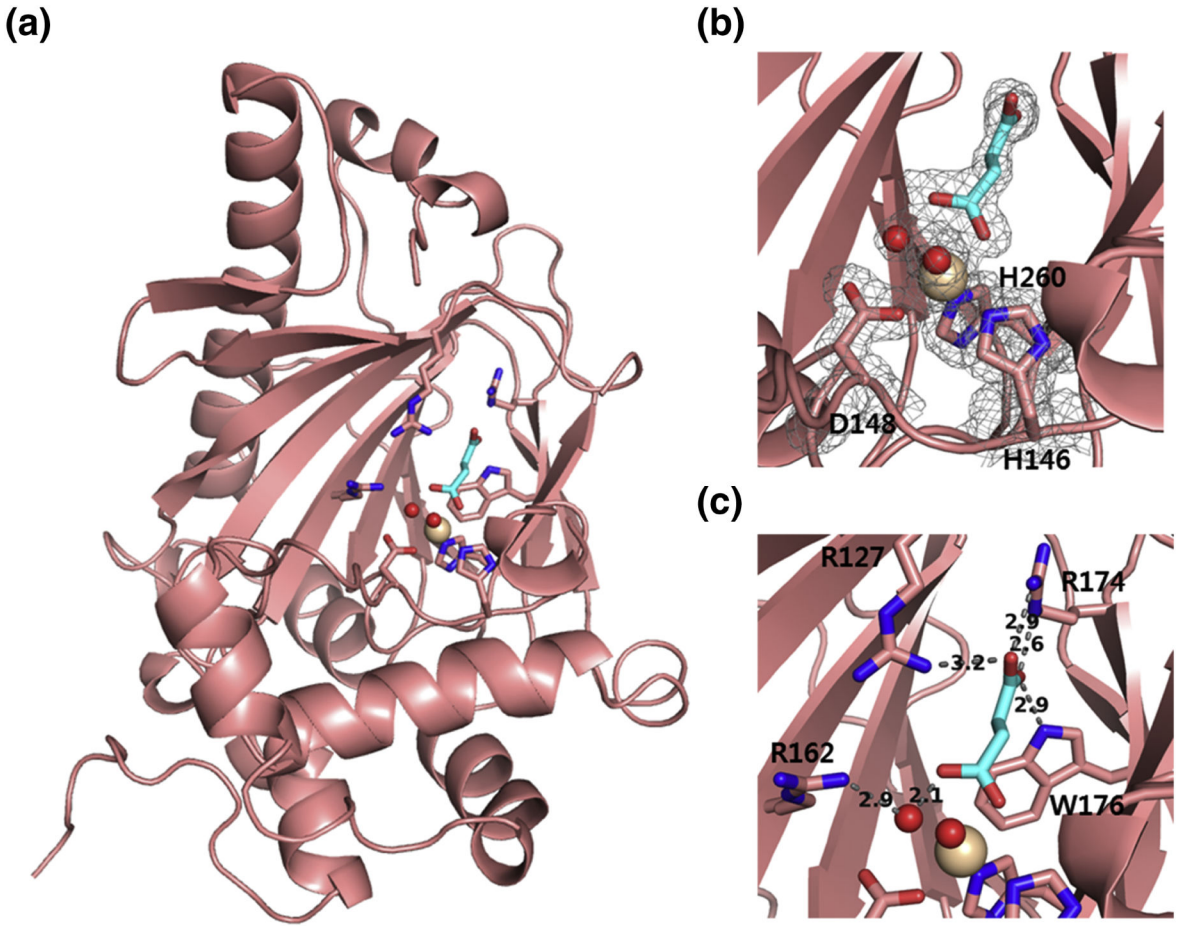

Figure 6.

Residues Arg127, Arg174 and Trp176 directly involved in the succinate binding of $KdoO_{MI}$/succinate/Fe(III) complex (salmon). (A) Fe(III) and succinate bound $KdoO_{MI.}$ (B) Corresponding simulated annealing omit electron density (gray mesh) for His146, Asp148, His260, Fe(III), water, and succinate was calculated with coefficients $2\mathbf{F}_o - \mathbf{F}_c$, contoured at 1 σ. (C) Close-up of the Fe(III)/succinate binding site. Salt bridges and hydrogen bonds between succinate and $KdoO_{MI}$ are indicated with dashed lines, along with their distances. Fe(III) (wheat sphere), succinate (cyan stick), and water (red non-bonded sphere) in $KdoO_{MI}$/succinate/Fe(III) complex are shown.

Table 1:

Purification table of $KdoO_{MI}$ in amounts and activities of the protein.

Fraction	Total Protein (mg)	Total activity (nmol/min)	%	Specific activity (nmol/min/mg)	X-fold purification
Cell Free (1)	1855	6432	100	3.5 ± 2.0	1
Cytosol (2)	1509	1870	29	1.2 ± 0.8	0.4
EDTA wash (3)	94	-	-	-	-
Membrane (4)	273	2761	43	10 ± 5	2.9
Soluble (5)	290	2520	39	9 ± 4	2.6
Insoluble (6)	63	45	0.7	0.7 ± 0.2	0.2
After Ni-NTA column (7)	31	4032	63	140 ± 42	40
After Size Exclusion column (8)	23	2766	43	120 ± 30	34

Table 2:

Data Collection and Refinement Statistics of $KdoO_{MI}$ (apoprotein) and $KdoO_{MI}$/Co(II) complex (Co(II)).

	$KdoO_{MI}$		
	Co(II), Phasing	**Apoprotein**	**Co(II)**
Data Collection			
Space group	$P2_12_12_1$	$P2_12_12_1$	$P2_12_12_1$
Unit cell(Å)	46.3, 59.66, 116.9	45.9, 59.5, 116.3	45.8, 59.6, 116.4
Wavlength (Å)	1.5	1.0	1.0
Resolution[a] (Å)	50–1.90 (1.93–1.90)	50–1.94 (1.97–1.94)	50–1.45 (1.48–1.45)
R_{merge}[a,b](%)	8.2 (30.8)	9.7 (28.1)	11.6 (45.4)
Mean $I/\sigma(I)$[a]	28.1 (3.7)	28.8 (5.2)	21.4 (2.4)
Completeness[a](%)	99.0 (85.5)	99.3 (87.1)	99.8 (98.1)
Redundancy[a]	9.4 (4.9)	7.0 (5.2)	7.0 (5.4)
Observed reflections (unique)	245,036 (25,986)	169,475 (24,341)	401,450 (57,453)
Correlation coefficient (%)	73		
Wilson B-factor		18.2	14.4
Refinement			
R_{factor}/R_{free}[c] (%)		15.7/20.5	15.7/17.9
protein residues per asu		297	297
water molecules per asu		252	274
other ligands per asu			
Chloride/Sulfate/Acetate		0/1/3	2/4/4
PG4/GOL/Metal/AKG/SIN		1/0/0/0/0	8/1/1/0/0
Ramachandran Plot			
Favored/allowed/outlier (%)		98.0/1.7/0.3	98.7/1.0/0.3
Rms deviations			
Bond length (Å)		0.006	0.005
Bond angles (°)		0.767	0.816
Average B factor (Å^2)		23.95	24.0
Macromolecules		22.72	21.4
Ligands		48.56	52.88
Solvent		33.04	35.44
PDB code		6A2E	5YKA

[a] Number in parentheses indicate the outer-resolution shell

[b] $\mathbf{R}_{\text{merge}} = \left[\sum_{\mathbf{hkl}}\sum_{\mathbf{i}}\left|\mathbf{I} - \langle\mathbf{I}\rangle\right| / \sum_{\mathbf{hkl}}\sum_{\mathbf{I}}\left|\mathbf{I}\right| \times 100\right]$.

[c] $\mathbf{R}_{\text{factor}}/\mathbf{R}_{\text{free}} = \sum_{\mathbf{hkl}}\left\|\mathbf{F}_{\text{O}}\right| - \left|\mathbf{F}_{\text{C}}\right\| / \sum_{\mathbf{hkl}}\left|\mathbf{F}_{\text{O}}\right|$, where $\mathbf{F}_{\text{O}}$ and $\mathbf{F}_{\text{C}}$ are the observed and calculated structure factors, respectively.

Table 3:

Data Collection and Refinement Statistics of $KdoO_{MI}$/α-KG/Fe(III) (Fe(III)- αKG) and $KdoO_{MI}$/succinate/Fe(III) (Fe(III)-succinate) complexes.

	$KdoO_{MI}$	
	Fe(III)-αKG	**Fe(III)-succinate**
Data Collection		
Space group	$P2_12_12_1$	$P2_12_12_1$
Unit cell(Å)	45.7, 59.2, 116.3	45.7, 59.3, 116.2
Wavlength (Å)	1.0	1.0
Resolution[a] (Å)	50–1.60(1.63–1.60)	50–1.49 (1.52–1.49)
R_{merge} [a,b](%)	10.4 (46.8)	8.3 (45.6)
Mean $I/\sigma(I)$ [a]	28.1 (3.3)	27.1 (2.3)
Completeness[a](%)	98.2 (86.5)	95.5 (77.0)
Redundancy[a]	10.0 (7.3)	5.9 (5.2)
Observed reflections (unique)	416,921 (41,701)	298,290 (50,288)
Wilson B-factor	18.6	16.6
Refinement		
R_{factor}/R_{free}[c](%)	16.0/18.2	16.7/18.3
protein residues per asu	294	293
water molecules per asu	166	222
other ligands per asu		
Chloride/Sulfate/Acetate	3/3/6	0/0/4
PG4/GOL/Metal/AKG/SIN	4/1/1/1/0	5/1/1/0/1
Ramachandran Plot		
Favored/allowed/outlier (%)	99.0/0.7/0.3	99.0/0.7/0.3
Rms deviations		
Bond length (Å)	0.005	0.005
Bond angles (°)	0.790	0.790
Average B factor (Å^2)	29.51	26.23
Macromolecules	28.08	24.65
Ligands	54.47	48.79
Solvent	39.18	35.91
PDB code	5YVZ	5YW0

[a] Number in parentheses indicate the outer-resolution shell

[b] $\mathbf{R}_{\text{merge}} = \left[\sum_{\mathbf{hkl}}\sum_{\mathbf{i}}\left|\mathbf{I} - \langle\mathbf{I}\rangle\right| / \sum_{\mathbf{hkl}}\sum_{\mathbf{I}}\left|\mathbf{I}\right| \times 100\right]$.

[c] $\mathbf{R}_{\text{factor}}/\mathbf{R}_{\text{free}} = \sum_{\mathbf{hkl}}\left\|\mathbf{F}_{\text{O}}\right| - \left|\mathbf{F}_{\text{C}}\right\| / \sum_{\mathbf{hkl}}\left|\mathbf{F}_{\text{O}}\right|$, where $\mathbf{F}_{\text{O}}$ and $\mathbf{F}_{\text{C}}$ are the observed and calculated structure factors, respectively.

Table 4.

Specific activities of variant forms of $KdoO_{MI}$ and percentiles relative to the wild-type enzyme

		Specific activity (nmol/min/mg)	% activity
$KdoO_{MI}$	WT	152 ± 35	100.0
	R127A	2.5 ± 0.5	1.6
	R162A	2.3 ± 0.2	1.5
	R174A	ND*	ND*
	W176A	62 ± 4	40.8
	H225A	27 ± 15	17.8

*ND: Not detected